Appl. Math. Mech. -Engl. Ed., **41**(3), 491–506 (2020)

Applied Mathematics and Mechanics (English Edition)

https://doi.org/10.1007/s10483-020-2583-9

Stochastic and upscaled analytical modeling of fines migration in porous media induced by low-salinity water injection*

Yulong YANG[1], Weifeng YUAN[1], Jirui HOU[1], Zhenjiang YOU[2,†], Jun LI[3], Yang LIU[3]

1. Unconventional Petroleum Research Institute, China University of Petroleum, Beijing 102249, China;
2. School of Chemical Engineering, The University of Queensland, Brisbane QLD 4072, Australia;
3. College of Petroleum Engineering, China University of Petroleum, Beijing 102249, China

(Received Sept. 9, 2019 / Revised Nov. 27, 2019)

Abstract Fines migration induced by injection of low-salinity water (LSW) into porous media can lead to severe pore plugging and consequent permeability reduction. The deep-bed filtration (DBF) theory is used to model the aforementioned phenomenon, which allows us to predict the effluent concentration history and the distribution profile of entrapped particles. However, the previous models fail to consider the movement of the waterflood front. In this study, we derive a stochastic model for fines migration during LSW flooding, in which the Rankine-Hugoniot condition is used to calculate the concentration of detached particles behind and ahead of the moving water front. A downscaling procedure is developed to determine the evolution of pore-size distribution from the exact solution of a large-scale equation system. To validate the proposed model, the obtained exact solutions are used to treat the laboratory data of LSW flooding in artificial soil-packed columns. The tuning results show that the proposed model yields a considerably higher value of the coefficient of determination, compared with the previous models, indicating that the new model can successfully capture the effect of the moving water front on fines migration and precisely match the effluent history of the detached particles.

Key words low-salinity water (LSW) flooding, fines migration, stochastic model, downscaling, porous media, waterflooding front, exact solution

Chinese Library Classification O29
2010 Mathematics Subject Classification 97M50

* Citation: YANG, Y. L., YUAN, W. F., HOU, J. R., YOU, Z. J., LI, J., and LIU, Y. Stochastic and upscaled analytical modeling of fines migration in porous media induced by low salinity water injection. *Applied Mathematics and Mechanics* (*English Edition*), **41**(3), 491–506 (2020) https://doi.org/10.1007/s10483-020-2583-9

† Corresponding author, E-mail: zhenjiang.you@gmail.com

Project supported by the National Natural Science Foundation of China (Nos. 51804316, 51734010, and U1762211), the National Science and Technology Major Project of China (No. 2017ZX05009), and the Science Foundation of China University of Petroleum, Beijing (No. 2462017YJRC037)

Nomenclature

c,	suspended-particle concentration;
C,	dimensionless suspended-particle concentration;
C_{v},	coefficient of variation;
f_{a},	fractional flow through accessible pores;
f_{ns},	fractional flow through inaccessible pores;
F_{d},	drag force;
F_{e},	electrostatic force;
F_{g},	gravity;
F_{L},	lifting force;
h,	total pore concentration;
h_0,	initial total pore concentration;
H,	pore size distribution;
k,	permeability;
k_0,	initial permeability;
k_1,	conductance in single pore;
l,	porous space dispersivity;
l_{d},	level arm of drag force;
l_{n},	level arm of normal force;
L,	length of porous specimen;
r_0,	averaged radius of moving particles;
r_{p},	radius of pore;
r_{s},	radius of particle;
s_1,	cross area of single pore;
S,	dimensionless captured-particle concentration;
S_{cr},	dimensionless critical attached-particle concentration;
S_{r},	dimensionless attached-particle concentration;
t,	time;
t_0,	the moment corresponding to intersection of characteristic line and water front;
U,	Darcy velocity;
x,	linear coordinate;
α,	drift delay factor;
β,	power index;
γ,	salinity;
Λ,	dimensionless filtration coefficient;
σ,	captured-particle concentration;
σ_0,	initial captured-particle concentration;
σ_{r},	attached-particle concentration;
φ_0,	initial porosity;
φ_{a},	accessible porosity.

1 Introduction

Fines migration with consequent permeability reduction is a widely recognized phenomenon in petroleum and environmental processes, for instance, water flooding in geothermal and hydrocarbon reservoirs[1–4], the storage of fresh water in shallow aquifers[5], fluid leak-off in drilling operations[6], and others. The primary sources of removable fine particles in reservoirs are clays, e.g., kaolinite, chlorite, and illite, whereas quartz and silica particles may be mobilized in low-consolidated sandstones[7]. The prediction and mitigation of the formation of the damage induced by fines migration pose a serious engineering problem. The typical approach to evaluating and regulating the extent of fines migration stands on a mathematical modeling supported by laboratory studies.

Several studies have demonstrated that the occurrence of particle detachment can be attributed to the unbalanced torques (see Fig. 1) of the drag force F_{d} and the normal forces (the electrostatic force F_{e}, the lifting force F_{L}, and the gravity F_{g}) exerting on a particle[8–12]. The velocity of fluid is one of the main factors that affect the drag force, while salinity, temperature, and pH are the key parameters influencing the electrostatic force, which is the summation of the London-van der Waals force, the electrical double layer force, and the born repulsion force. Salinity contributes more to the variation of the double layer repulsion force arising from the overlap of the diffused double layers of ions around charged particles[4]. The torque balance criterion yields the maximum concentration σ_{cr} of particles adhering to surfaces under a certain fluid condition, i.e., $\sigma_{\mathrm{r}} = \sigma_{\mathrm{cr}}(U, \gamma, \mathrm{pH}, T)$, where σ_{r} represents the concentration of attached particles on rock surfaces. Bedrikovetsky et al.[13] derived a critical retention function assuming that mono-sized particles deposit layer by layer on the surface of a cylindrical pore, and Yang et al.[14] proposed another way to obtain the maximum retention concentration via the torque balance expression for one-layer attached particles that are distributed according to size. According to their study, the extra attached particles are released instantly after changing the

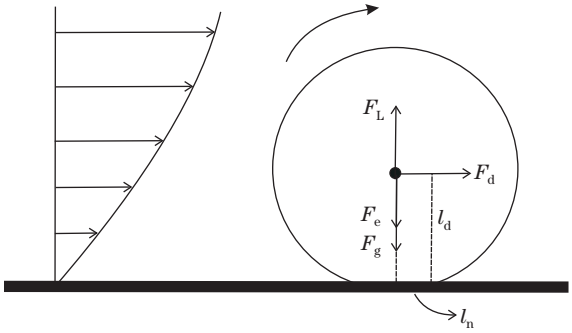

Fig. 1 Schematic of torques exerting on an attached particle

conditions of the fluid. However, Mahani et al.[15] claimed that the Nernst-Planck diffusion of ions could cause a significant delay of oil-droplet detachment when low-salinity water (LSW) is introduced into the system. The same effect might also be expected for clay-particle remobilization in LSW flooding. Yet, few papers present a quantitative analysis of the influence of Nernst-Planck diffusion on fines detachment.

Based on the analogy of the deep-bed filtration (DBF) theory, the mathematical model for fines migration in porous media contains formulations of particle transport and plugging. Besides, a kinetic equation is introduced to quantify the process of particle detachment, in which the concept of maximum retention concentration is generally involved[13,16–17]. Yang and Bedrikovetsky[18] presented an exact solution for a fines migration problem, considering arbitrary accessibility and filtration functions. Galaguz and Safina[19] obtained the numerical solution for the same governing equation system with initially deposited particles. Borazjani et al.[20] derived an analytical model for two-phase flow, characterizing the effect of fines migration on LSW flooding. However, the aforementioned models assumed that the extra particles beyond the critical retention concentration are detached at the initial moment of injection and fail to consider the moving boundary of water flooding before the breakthrough of the injected water. Apparently, this assumption is questionable in modeling fines migration induced by LSW flooding as clay particles can only be released after the arrival of the injected LSW. The released particles give rise to a shock at the moving water front. We apply the Rankine-Hugoniot (RH) jump condition to address this discontinuity in the particle concentration. The RH condition, based on the conservation laws of mass, momentum, and energy, provides us a simple and straightforward method to obtain the values of shock parameters of practical applications[21].

Several laboratory studies reported a significant delay for the breakthrough of the fine particles removed by increasing the fluid velocity or decreasing salinity if compared with the arrival time of the tracers[22–24]. This hysteresis of fines migration is attributed to the slow movement of particles near the rock surface and is modeled by introducing a drift delay factor, which is defined by the ratio of the velocities of particles and fluid[14,19,25–26].

Particle straining or size exclusion during filtration depends on the ratio of particles and pore sizes. A stochastic model based on the particle DBF theory has been developed, accounting for particle- and pore-size distributions[27]. Bedrikovetsky[28] introduced the flux reduction factor, which characterizes the fractional flow via accessible pores, while the rate of particle straining is proportional to the flux through inaccessible pores. The stochastic model can be upscaled for the flow of mono-sized particle suspension in porous media with variant pore sizes, and the exact-solution-based downscaling process allows us to determine the variations in pore size distributions, which have a significant impact on particle filtration in porous media[25]. The stochastic model for DBF can be applied in the fines migration problem by modifying the initial and boundary conditions. Yet, the stochastic-model-based upscaling and the exact-

solution-based downscaling procedures for fines migration are not available in literature.

In the current study, we present a stochastic model for fines migration during LSW flooding and its upscaling in the case of mono-sized moving particles. The RH condition is used to quantify the removed particle concentration at the moving boundary of the LSW front. The derived exact solutions of the analytical model determine the evolution of pore size distribution by inversely tuning the experimental data (downscaling).

The structure of the text is as follows. Section 2 presents the mathematical model for fines migration, including the formulation of the upscaled governing equations from a stochastic model, the derivation of exact solutions, and the downscaling procedure to determine the evolution of pore size distribution. Section 3 discusses the general behavior of the obtained exact solutions and the sensitivity analysis regarding tuning parameters. Section 4 presents the treatment of laboratory data using the analytical model. Section 5 concludes the paper.

2 Mathematical model

This section presents the mathematical model for straining-dominant migration of mono-sized fines in porous media with distributed pore sizes. Subsection 2.1 presents the governing equations upscaled from a population balance model, accounting for the depth filtration of mono-sized particles. Subsection 2.2 derives the exact solutions using the characteristic line method.

2.1 Governing equations

The flow region of porous media is simplified as a bundle of parallel cylinders with different radii intercalated by mixing chambers in the population balance model[28]. Size exclusion is the primary mechanism to capture moving particles through a straining-dominant filtration process in porous media, i.e., particles with a smaller size than the pores move freely through the tubes from one chamber to another, whereas larger particles are strained at the entrance of the pores (see Fig. 2).

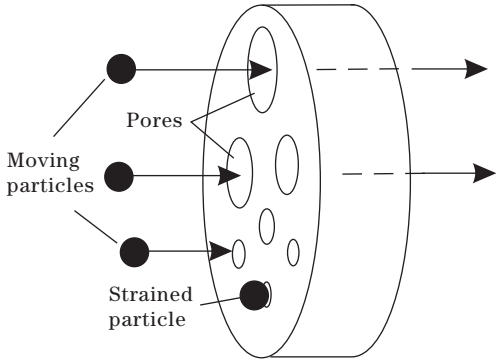

Fig. 2 Schematic of size exclusion effect

The detailed derivation of the microscale governing equation system accounting for the pore size $H(r_\mathrm{p}, x, t)$ and particle size $C(r_\mathrm{s}, x, t)$ distributions, including the mass balance equation of suspended and strained particles and the kinetic equations for pore plugging and particle capturing rates, can be found in Refs. [25] and [28]. r_p and r_s are pore and particle sizes, respectively. The number of all pores per unit cross area $h(x,t)$ is determined by integrating the pore size distribution function over pore size r_p, i.e., $h(x,t) = \int_0^\infty H(r_\mathrm{p}, x, t)\mathrm{d}r_\mathrm{p}$. Analogously, the overall concentration of the moving particles $c(x,t)$ is defined by $c(x,t) = \int_0^\infty C(r_\mathrm{s}, x, t)\mathrm{d}r_\mathrm{s}$, and the total concentration of the strained particles $\sigma(x,t)$ is calculated by $\sigma(x,t) = \int_0^\infty \Sigma(r_\mathrm{s}, x, t)\mathrm{d}r_\mathrm{s}$.

The suspension and retention concentrations of mono-sized particles can be expressed as $C(r_\mathrm{s}, x, t) = c(x,t)\delta(r_\mathrm{s} - r_0)$ and $\Sigma(r_\mathrm{s}, x, t) = \sigma(x,t)\delta(r_\mathrm{s} - r_0)$, respectively, which allows us to

find the upscaling of the population balance model, yielding the averaged macroscale governing equations[25,28],

$$\frac{\partial}{\partial t}(\varphi_{\mathrm{a}}[H]c(x,t)+\sigma_{\mathrm{r}}(x,t)+\sigma(x,t))+\alpha U\frac{\partial}{\partial x}(c(x,t)f_{\mathrm{a}}[H])=0, \tag{1}$$

$$\frac{\partial\sigma(x,t)}{\partial t}=\frac{1}{l}f_{\mathrm{a}}f_{\mathrm{ns}}[H]c(x,t)\alpha U, \tag{2}$$

$$\frac{\partial h(x,t)}{\partial t}=-\alpha U c(x,t)f_{\mathrm{a}}f_{\mathrm{ns}}[H]\equiv -l\frac{\partial\sigma(x,t)}{\partial t}, \tag{3}$$

where U is the Darcy velocity of fluid, σ_{r} is the concentration of attached particles on the rock surface, x is the spatial coordinate, t is the time coordinate, and φ_{a} is the accessible porosity, defined by $\varphi_{\mathrm{a}}[H]=\int_{r_{\mathrm{s}}}^{\infty}s_1(r_{\mathrm{p}})H(r_{\mathrm{p}},x,t)\mathrm{d}r_{\mathrm{p}}$, in which s_1 represents the area of one pore with the radius r_{p}. r_0 is the averaged size of moving particles, and f_{a} is the fractional flow through the accessible pores, expressed by $f_{\mathrm{a}}=\frac{1}{k}\int_{r_{\mathrm{s}}}^{\infty}k_1(r_{\mathrm{p}})H(r_{\mathrm{p}},x,t)\mathrm{d}r_{\mathrm{p}}$, in which $k_1(r_{\mathrm{p}})=\pi r_{\mathrm{p}}^4/8$ represents the conductance in a single pore, and k is the permeability of the porous media. f_{ns} is the fractional flow through the inaccessible pores. Apparently, $f_{\mathrm{ns}}=1-f_{\mathrm{a}}$. l is the inter-chamber distance or dispersivity determined by $l(r_{\mathrm{s}})=l_0f_{\mathrm{ns}}^{\beta}$, where l_0 and β are constant[25].

Integrating Eq. (3) over t yields

$$\frac{h}{l}+\sigma=\frac{h_0}{l}+\sigma_0, \tag{4}$$

where h_0 and σ_0 are the initial pore and strained-particle concentrations, respectively.

Assume that the pore concentration is uniformly distributed along the distance at the initial moment, namely,

$$H(r_{\mathrm{p}},x,t)=H_0(r_{\mathrm{p}})\quad\text{at}\quad t=0. \tag{5}$$

The pore concentration distribution function $H(r_{\mathrm{p}},x,t)$ can be expressed by $H(r_{\mathrm{p}},y)$[28],

$$H(r_{\mathrm{p}},y(h))=H_0(r_{\mathrm{p}})\mathrm{e}^{-k_1(r_{\mathrm{p}})y(h)}, \tag{6}$$

where $y(h)$ is obtained from

$$h(y)=\int_0^{\infty}H_0(r_{\mathrm{p}})\mathrm{e}^{-k_1(r_{\mathrm{p}})y(h)}\mathrm{d}r_{\mathrm{p}}. \tag{7}$$

When $y=0$, from Eqs. (6) and (7), $H=H_0(r_{\mathrm{p}})$, and $h=h_0$.

Introducing the following dimensionless parameters into Eqs. (1)–(2):

$$x\to\frac{x}{L},\quad t\to\frac{Ut}{\varphi_0L},\quad C=\frac{c\varphi_0}{\Delta\sigma_{\mathrm{r}}},\quad S=\frac{\sigma}{\Delta\sigma_{\mathrm{r}}},\quad S_{\mathrm{r}}=\frac{\sigma_{\mathrm{r}}}{\Delta\sigma_{\mathrm{r}}},\quad s=\frac{\varphi_{\mathrm{a}}}{\varphi_0} \tag{8}$$

yields the dimensionless forms of the governing equations,

$$\frac{\partial}{\partial t}(s(S)C+S_{\mathrm{r}}+S)+\alpha\frac{\partial}{\partial x}(Cf_{\mathrm{a}}(S))=0, \tag{9}$$

$$\frac{\partial S}{\partial t}=\alpha\Lambda(S)C, \tag{10}$$

$$\Lambda(S)=Lf_{\mathrm{a}}f_{\mathrm{ns}}/l, \tag{11}$$

where L is the core length, φ_0 is the initial porosity, $\Delta\sigma_{\mathrm{r}}$ is the removed particle concentration when the LSW front arrives at a certain location, C is the dimensionless suspension

concentration, S is the dimensionless strained-particle concentration, S_{r} is the dimensionless attached-particle concentration on rock surfaces, and $\Lambda(S)$ is the dimensionless filtration coefficient.

We assume that all the fine particles are attached to the rock surface initially, or in other words, the porous media are free of suspended or strained particles. It is also assumed that the porous media are saturated with water, and the salinity and attached-particle concentrations are constant along the distance. Therefore, we have

$$C = S = 0, \quad \Gamma = 1, \quad S_{\mathrm{r}} = S_{\mathrm{cr}}\ (\Gamma = 1) \quad \text{at} \quad t = 0, \tag{12}$$

where $t = 0$ represents the initial moment, and Γ denotes the dimensionless salinity, defined by $\Gamma = (\gamma - \gamma_{\mathrm{inj}})/(\gamma_0 - \gamma_{\mathrm{inj}})$, in which γ is salinity, γ_{inj} is the salinity of the injected fluid, and γ_0 is the initial salinity. Therefore, $\Gamma = 1$ stands for the initial salinity, and $S_{\mathrm{cr}}\ (\Gamma = 1)$ represents the maximum retention concentration at $\Gamma = 1$.

Particle-free LSW is injected into the porous media, and therefore, the boundary conditions at the core inlet are expressed as

$$C = \Gamma = 0 \quad \text{at} \quad x = 0. \tag{13}$$

$\Gamma = 0$ represents the dimensionless salinity of the injected water.

Neglecting the diffusion effect, the salinity ahead of the flooding front is the original salinity in the porous media, and the salinity behind the flooding front equals the injected value, i.e.,

$$\Gamma(x,t) = \begin{cases} 1, & x > t, \\ 0, & x \leqslant t. \end{cases} \tag{14}$$

We assume that the excess particles after the injection of LSW are detached immediately when the flooding front arrives at a certain distance. As a result, the concentration of the attached particles is constant both behind and ahead of the front. Then, Eq. (9) can be simplified as

$$\frac{\partial}{\partial t}(s(S)C + S) + \alpha\frac{\partial}{\partial x}(Cf_{\mathrm{a}}(S)) = 0. \tag{15}$$

At the water flooding front, the conservation of particle concentration is expressed by the RH condition,

$$(s(S)C + S + S_{\mathrm{r}}(\Gamma))D = [\alpha f_{\mathrm{a}}(S)C]. \tag{16}$$

In Eq. (16), the square bracket [ ] denotes the jump of a physical parameter behind and ahead of the flooding front, i.e., $[A] = A^+ - A^-$. The symbol "+" indicates a position ahead of the front, while "−" denotes a position behind the front. D represents the speed of the flooding front. At $x = t$, we have

$$C^+ = 0, \quad S^+ = S^- = 0, \quad S_{\mathrm{r}}^+ = S_{\mathrm{cr}}\ (\Gamma = 1), \quad S_{\mathrm{r}}^- = S_{\mathrm{cr}}\ (\Gamma = 0), \quad D = 1. \tag{17}$$

Substituting Eq. (17) into Eq. (16), one obtains the suspension concentration behind the moving front,

$$C^- = \frac{\Delta S_{\mathrm{r}}}{s(0) - \alpha f_{\mathrm{a}}(0)}, \tag{18}$$

where $\Delta S_{\mathrm{r}} = S_{\mathrm{cr}}\ (\Gamma = 1) - S_{\mathrm{cr}}\ (\Gamma = 0)$, which gives the amount of detached particles when the LSW front arrives at x. Apparently, ΔS_{r} equals one according to the definition of the dimensionless retention concentration. $s(0)$ and $f_{\mathrm{a}}(0)$ represent the values of s and f_{a} when $S = 0$, respectively.

Equation (18) is considered as the moving boundary condition of the suspended-particle concentration behind the front of the water flooding.

2.2 Exact solutions

The overall flow region can be divided into three zones (see Fig. 3(a)): the area ahead of the waterflood front (Zone I), the area between the waterflood front and the rear front of particle transportation (Zone II), and the area behind the rear front of particle transportation (Zone III).

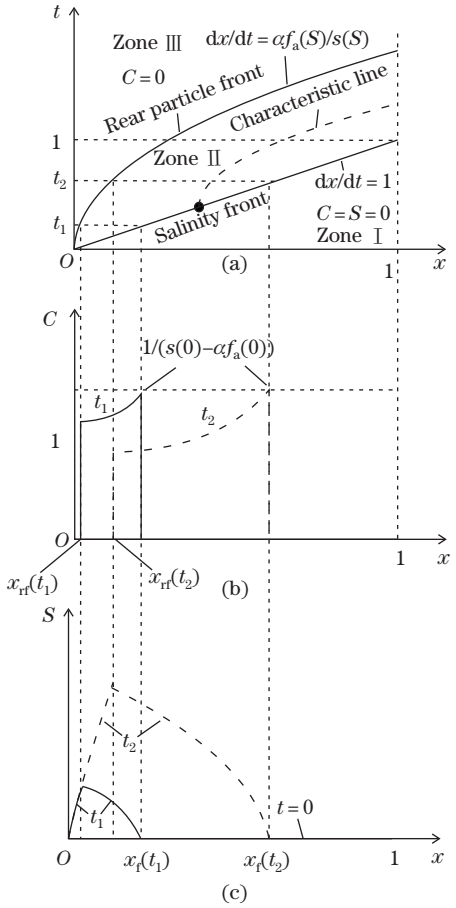

Fig. 3 Schematic of exact solutions

2.2.1 Zone I

We first derive solutions ahead of the waterflood front, i.e., $x > t$. Substituting Eqs. (10) and (11) into Eq. (15), we obtain

$$s(S)\frac{\partial C}{\partial t} + \alpha f_{\mathrm{a}}(S)\frac{\partial C}{\partial x} = -\Big(\frac{\partial s(S)}{\partial t} + \frac{\partial \alpha f_{\mathrm{a}}(S)}{\partial x}\Big)C - \alpha\Lambda(S)C. \tag{19}$$

The exact solution to Eq. (19) can be derived by using the characteristic line method. According to Eq. (12), the suspension concentration is zero in Zone I, where the LSW front has not arrived yet, i.e., when $x > t, C = 0$. Therefore, following Eq. (10), the concentration of strained particles is also zero in this region, i.e., when $x > t, S = 0$. The corresponding formulae are listed in the second column of Table 1.

Table 1 Exact solutions for migration of detached particles during LSW flooding

Variable	$t < x$	$x < t < t_{\rm rf}$	$t > t_{\rm rf}$
Γ	1	0	0
$S_{\rm r}$	$S_{\rm r}$ ($\Gamma = 1$)	$S_{\rm r}$ ($\Gamma = 0$)	$S_{\rm r}$ ($\Gamma = 0$)
C	0	$\dfrac{1}{\alpha\Lambda(S)}\dfrac{\partial S}{\partial t}$	0
S	0	$\displaystyle\int_0^S \frac{\alpha f_{\rm a}(S) - s(S)}{\alpha\Lambda(S)(\Delta S_{\rm r} - S)}{\rm d}S = x - t$	$S_{\rm r}(x, t_{\rm rf}(x))$

2.2.2 Zone II

We now derive solutions for the region between the waterflood front and the rear front of particle transportation.

From Eq. (10), we have

$$C = \frac{1}{\alpha\Lambda(S)}\frac{\partial S}{\partial t} = \frac{\partial F(S)}{\partial t}, \tag{20}$$

where

$$F(S) = \int_0^S \frac{1}{\alpha\Lambda(u)}{\rm d}u. \tag{21}$$

Substituting Eq. (20) into Eq. (15), we obtain

$$\frac{\partial}{\partial t}\Big(s(S)\frac{\partial F(S)}{\partial t} + S\Big) + \alpha\frac{\partial}{\partial x}\Big(\frac{\partial F(S)}{\partial t}f_{\rm a}(S)\Big) = 0. \tag{22}$$

Changing the order of differentiation over x and t in the second term of Eq. (22) and integrating in t yield

$$s(S)\frac{\partial F(S)}{\partial t} + S + \alpha f_{\rm a}(S)\frac{\partial F(S)}{\partial x} = \Big(s(S)\frac{\partial F(S)}{\partial t} + S + \alpha f_{\rm a}(S)\frac{\partial F(S)}{\partial x}\Big)_{x=t}, \tag{23}$$

i.e., the value of the left-hand side of Eq. (23) is equal to its value along the front $x = t$.

Let us calculate the right-hand side of Eq. (23). Along the salinity front, we have $S = 0$. Thus,

$$\Big(\frac{\partial S}{\partial t} + \frac{\partial S}{\partial x}\Big)_{x=t} = 0. \tag{24}$$

The suspended concentration is equal to C^- behind the salinity front. As it follows from Eq. (10),

$$\frac{\partial S}{\partial t}\Big|_{x=t} = \alpha\Lambda(0)\frac{\Delta S_{\rm r}}{s(0) - \alpha f_{\rm a}(0)}. \tag{25}$$

Substituting Eqs. (24) and (25) into Eq. (23), we obtain

$$\frac{s(S)}{\alpha\Lambda(S)}\frac{\partial S}{\partial t} + \frac{f_{\rm a}(S)}{\Lambda(S)}\frac{\partial S}{\partial x} = \Delta S_{\rm r}. \tag{26}$$

The characteristic line is determined by

$$\frac{{\rm d}x}{{\rm d}t} = \frac{\alpha f_{\rm a}(S)}{s(S)}. \tag{27}$$

Integrating Eq. (26) along characteristic lines yields

$$\int_0^S \frac{s(S)}{\alpha\Lambda(S)(\Delta S_\mathrm{r}-S)}\mathrm{d}S = t - t_0. \tag{28}$$

Here, the characteristic lines are parameterized by time t, and t_0 corresponds to the moment at the crossing of the characteristic line and the salinity front (see Fig. 3(a)). Parameterizing the characteristic lines by the coordinate x in Eq. (26) and integrating over x from t_0 to x result in

$$\int_0^S \frac{f_\mathrm{a}(S)}{\Lambda(S)(\Delta S_\mathrm{r}-S)}\mathrm{d}S = x - t_0. \tag{29}$$

Excluding t_0 from Eqs. (28) and (29) yields the implicit expression for the solution $S(x,t)$,

$$\int_0^S \frac{s(S)}{\alpha\Lambda(S)(\Delta S_\mathrm{r}-S)}\mathrm{d}S - t = \int_0^S \frac{f_\mathrm{a}(S)}{\Lambda(S)(\Delta S_\mathrm{r}-S)}\mathrm{d}S - x. \tag{30}$$

The corresponding formulae are listed in the third column of Table 1.

2.2.3 Zone III

The particle rear front corresponds to the characteristic line starting from $t_0 = 0$. As it follows from Eqs. (28) and (29), the front trajectory $t_\mathrm{rf}(x)$ is determined from

$$\int_0^S \frac{s(S)}{\alpha\Lambda(S)(\Delta S_\mathrm{r}-S)}\mathrm{d}S = t_\mathrm{rf}(x), \quad \int_0^S \frac{f_\mathrm{a}(S)}{\Lambda(S)(\Delta S_\mathrm{r}-S)}\mathrm{d}S = x. \tag{31}$$

Behind the rear front, the suspension concentration is determined using Eq. (19) with the boundary conditions (12). Therefore, we have $C = 0$ in this zone. The strained-particle concentration behind the rear front reaches a steady state after $t_\mathrm{rf}(x)$, the moment when the rear front passes by x. The corresponding formulae are listed in the fourth column of Table 1.

2.3 Downscaling: evolution of pore size distribution during the mono-sized fines migration

This section derives the downscaling of the analytical model obtained in Subsections 2.1 and 2.2 for mono-sized fines migration in porous media, retrieving the evolutionary history of the pore size distribution during particle straining.

The exact solutions, Eq. (30) for $S(x,t)$ and Eq. (20) for $C(x,t)$, are expressed via the model functions $s(S)$, $f_\mathrm{a}(S)$, and $\Lambda(S)$, which in turn are defined via the pore size distribution $H(r_\mathrm{p},x,t)$, as presented in Subsection 2.1. The variations of the three model functions with increasing S for three particle sizes are shown in Fig. 4. A larger particle size yields a lower accessibility $s(S)$ and a lower fractional flow $f_\mathrm{a}(S)$ through accessible pores. The accessibility remains constant as S increases because large pores cannot be plugged according to the size exclusion effect. With the accumulation of strained particles, the fractional flow tends to one, when all smaller pores disappear, and particles transport freely without being captured. In comparison, the filtration coefficient exhibits a more complicated behavior. As shown in Eq. (11), $\Lambda(S)$ is a non-monotonous function of f_a and is determined by a competitive effect of f_a and f_ns.

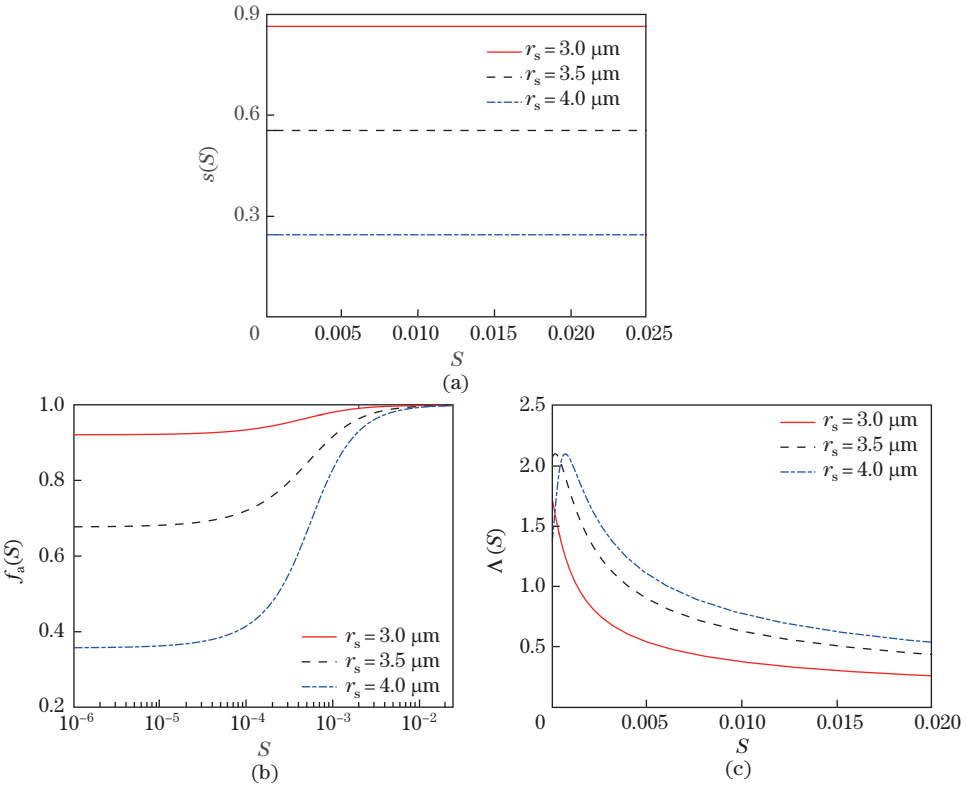

Fig. 4 Model functions for three particle sizes: (a) accessibility $s(S)$, (b) fractional flow $f_a(S)$, and (c) filtration coefficient $\Lambda(S)$

Equations (4)–(7) determine the evolution of pore size distribution via the solution $S(x,t)$ and the initial pore size distribution $H_0(r_p)$. Equation (6) provides a solution to the downscaling problem. Figure 5 shows the calculation for the pore size variation at the midpoint of a core at different moments. As expected, the pores whose sizes are larger than the mean particle size remain invariable, while the pores whose sizes are smaller than the mean particle size decrease with the increasing time.

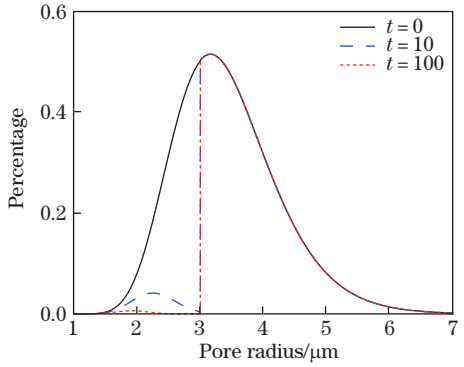

Fig. 5 Calculation example of the evolution of pore size distribution

3 Qualitative analysis of the exact solutions

3.1 General behavior of the exact solutions

Figure 3(a) shows a schematic diagram of the xt-plane, as well as the three regions for exact solutions divided by characteristic lines. Figures 3(b) and 3(c) display the profiles of suspension and strained-particle concentrations at moments t_1 and t_2.

The suspension concentration is zero behind the rear front of moving particles and ahead of the salinity front. Behind the salinity front, the suspension concentration monotonously increases from the rear particle front toward the salinity front. The value at the rear front decreases as time increases, whereas the suspension concentration at the salinity front remains the same, as given in Eq. (18).

According to the initial condition, Eq. (12), the strained-particle concentration starts from zero, i.e., the origin. Its value remains zero at the core inlet, which can be obtained by substituting the boundary condition of suspension concentration of Eq. (13) into the kinetic equation for the particle straining rate (see Eq. (10)). Ahead of the moving salinity front, the strained concentration is also zero because of the absence of suspended particles. Behind the rear moving front of particles, the strained concentration maintains the value of $S(x, t_{\mathrm{rf}}(x))$, which increases monotonically with x because of the continuous exposure (at a further distance) to the suspended particles transported from upstream. At a certain moment, the strained concentration decreases monotonically along x ahead of the rear particle front because the position where the rear front arrives gets accumulated by strained particles first compared with other points, and therefore, the strained concentration becomes maximum at the rear particle front.

3.2 Sensitivity analysis

We assume that the initial pore sizes follow a log-normal distribution, which is defined by the coefficient of variation C_{v} and the mean pore size $\langle r_{\mathrm{p}} \rangle$[17]. These two parameters, along with the drift delay factor α, are considered as tuning parameters. To further demonstrate the behavior of the model, the sensitivity analysis regarding the three tuning parameters is performed. Unless otherwise stated, other model parameters are $r_{\mathrm{s}} = 3\,\square\mathrm{m}$, $l_0 = 0.006\,5$, $\beta = 0.58$, and $\Delta\sigma_{\mathrm{r}} = 10^7$.

Figures 6(a)–6(c) depict the variations in the outlet concentration with the corresponding parameters, where PVI means pore volume injection. In Fig. 6(a), we observe that increasing the mean pore size results in a higher breakthrough concentration. This can be explained by the size exclusion effect, which is the main assumption of our model. Larger pore sizes also lead to a slight delay of the breakthrough time because of the competitive effect of the fractional flow f_{a} and the dimensionless porosity φ_{a}. These two parameters can influence the moving speed of remobilized particles, as expressed by Eq. (27). As shown in Fig. 6(b), a larger C_{v} yields a slightly lower breakthrough concentration as a wider size distribution indicates that there are more pores whose sizes are smaller than particles, and therefore, more particles remain trapped in the porous media. However, the model is not sensitive to the variation of C_{v}. Figure 6(c) shows the sensitivity of the drift delay factor. As expected, a low drift delay factor yields a later breakthrough because of the slow fines migration.

4 Experimental data treatment

The laboratory data used for model validation are obtained from the previous studies[29]. The authors performed LSW flooding tests on an artificial column packed with non-calcareous soil materials containing 16% sand, 18% clay, and 66% loam. The columns were initially saturated with 0.5 mol/L NaCl solution, and then, low-salinity solutions of 0.01 mol/L, 0.02 mol/L, and 0.04 mol/L were injected for each test. The details of the experiments are provided in Ref. [29].

Three unknown tuning parameters, C_{v}, $\langle r_{\mathrm{p}} \rangle$, and α, are inversely determined by optimizing

the history of breakthrough concentrations of remobilized particles. The improved Levenberg-Marquardt algorithm in MATLAB is used to minimize the difference between the model prediction and experimental data. This algorithm acts as the gradient-descent method if the initial parameters are far from the optimal value, and works as the Gauss-Newton method if the initial parameters are close to the optimal value. The tuning results of each test are listed in Table 2.

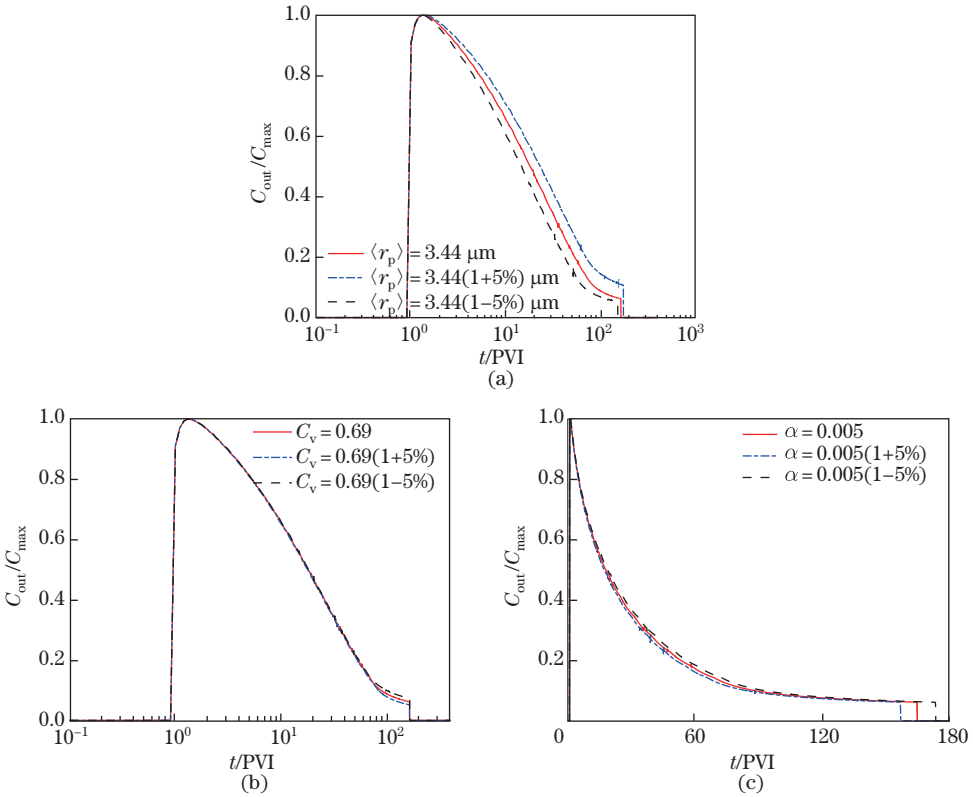

Fig. 6 Sensitivity of effluent particle concentration of particles with respect to 5% variation of parameters: (a) mean pore size $\langle r_p \rangle$, (b) coefficient of variation C_v, and (c) drift delay factor α

Table 2 Ion concentration and tuning results for each test

$Na^+/(mmol \cdot L^{-1})$	Tuning parameter		
	$\langle r_p \rangle$	C_v	α
10	3.04	0.49	1.0×10^{-2}
20	3.44	0.69	5.0×10^{-3}
40	3.13	0.69	1.1×10^{-3}

Figures 7(a)–7(c) compare the results of data treatment with the present model and the model previously developed by Yang and Bedrikovetsky[18]. We refer to the previous model as "YB model". The blue dots denote the laboratory data of the effluent concentration of mobilized clay particles, the red solid curves show the modeling results of the current model, and the green dashed lines present the modeling results of the YB model.

As shown by the experimental data, the effluent concentration starts to increase after one PVI. This is explained by the travelling time of the LSW flooding front, i.e., the moving front arrives at the outlet after 1 PVI. At 2–5 PVIs, the effluent concentration reaches its maximum level and then declines gradually till at more PVIs. The latter indicates a noticeable delay

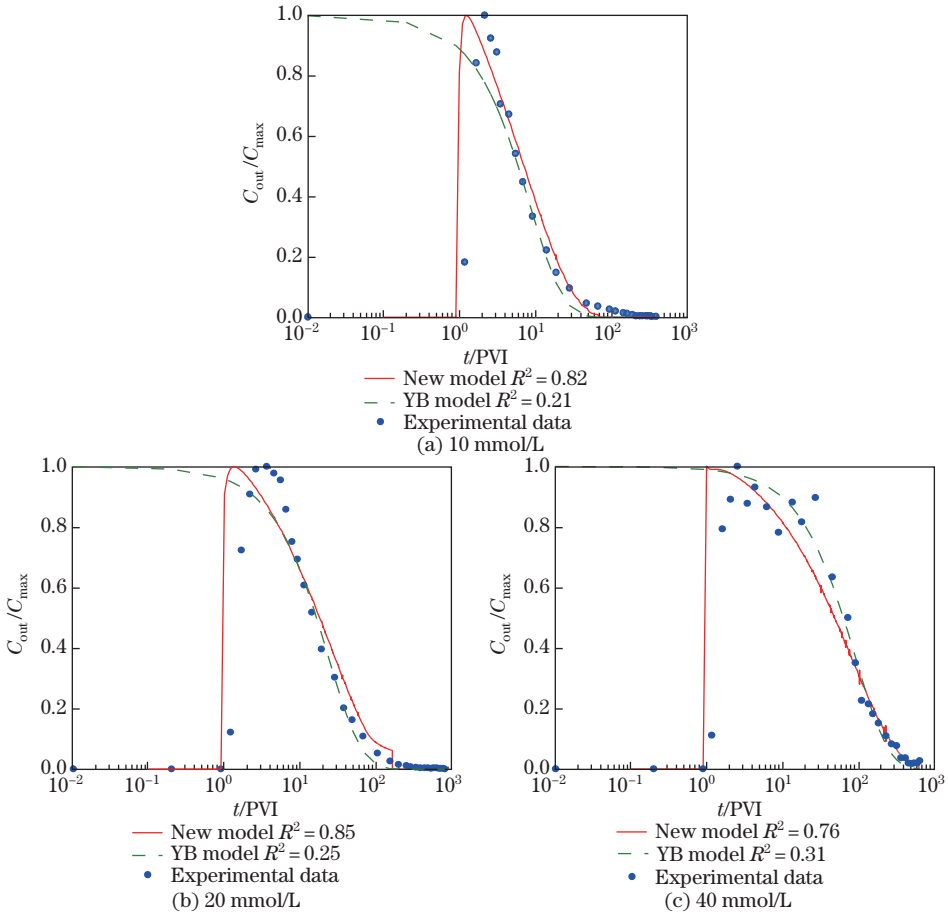

Fig. 7 Data treatment of effluent particle concentration in the presence of variant Na^+ concentrations by the current model and the YB model[19]

of the moving particles compared with the fluid. This hysteresis can be attributed to the following reasons. First, the remobilization of particles exposed to LSW occurs with a delay because of the Nernst-Planck diffusion of ions in the channel between the particles and the rock surface[15]. Meanwhile, the heterogeneity of rock surfaces and the clay particles with different components and sizes may also lead to distributed rates of detachment, which can be mathematically described by using the Taylor series expansion of the attached concentration at $t = 0$. Second, as the fluid speed close to a surface is significantly lower than the average velocity, the removed particles exhibit a drift delay over the surface[19,24], which is characterized by the introduction of the drift delay factor α in our model. The tortuosity of the flow path in a porous medium may also contribute to the drift delay of particles. As depicted by the green lines of each graph of Fig. 7, the YB model fails to consider the moving front. In the YB model, we assume that the LSW fills the whole core instantly after injection. As a result, the removed particles flow out of the core immediately. It is also assumed that the effluent concentration is equal to that of the detached particles at the initial moment, i.e., $(C_{out}/C_{max})_{t=0} = 1$, which contradicts to what has been observed in the experiments. In comparison, the model derived in this study successfully describes the process of remobilized-fines migration before the arrival of the LSW front by applying the RH condition at the moving boundary. As expected, the newly developed model largely agrees with the modeling and experimental data, and the coefficient of determination can reach between 0.76 and 0.85; optimizations using the YB model give

the values of the coefficient of determination ranging from 0.21 to 0.44, signifying inadequate treatments.

5 Concluding remarks

The exposure of clay particles to LSW enhances the double-layer repulsion force between the particles and the rock surfaces. Therefore, the particles initially attached to the rock surfaces are detachable under the shearing of fluid during LSW flooding, which may result in consequent pore plugging and permeability decline in the porous media.

We develop a stochastic model to characterize the process of fines migration in the porous media during LSW flooding, accounting for the movement of flooding front. The RH condition is successfully used to determine the moving boundary condition of the suspension concentration, and a drift delay factor is introduced to delineate the slow migration of remobilized fines.

Exact solutions of the proposed analytical model are derived based on the characteristic lines. A downscaling procedure is also formulated, which allows us to determine the evolution of pore size distribution from the exact solution of the large-scale equation system. Sensitivity analysis shows that the model is less sensitive to the coefficient of variation compared with the mean pore size and the drift delay factor.

The treatment of the experimental data of the effluent particle concentration during the injection of LSW is performed by using the proposed model and the previous YB model. The comparison demonstrates significant advantages of the newly developed model when the moving front is considered, and its exact solution exhibits close agreement with the experimental flooding data.

Acknowledgements The authors are grateful to Professor P. BEDRIKOVETSKY (The University of Adelaide) for the discussion of the analytical model.

References

[1] KHILAR, K. C. and FOGLER, H. S. *Migrations of Fines in Porous Media*, Kluwer Academic Publishers, Dordrecht (1998)

[2] MOGHADASI, R., ROSTAMI, A., HEMMATI-SARAPARDEH, A., and MOTIE, M. Application of nanosilica for inhibition of fines migration during low salinity water injection: experimental study, mechanistic understanding, and moder development. *Fuel*, **242**, 846–862 (2019)

[3] OCHI, J. and VERNOUX, J. F. A two-dimensional network model to simulate permeability decrease under hydrodynamic effect of particle release and capture. *Transport in Porous Media*, **37**(3), 303–325 (1999)

[4] YOU, Z., BADALYAN, A., YANG, Y., BEDROKOVETSKY, P., and HAND, M. Fines migration in geothermal reservoirs: laboratory and mathematical modelling. *Geothermics*, **77**(3), 344–367 (2019)

[5] PROMMER, H., DESCOURVIERES, C. D., HANDYSIDE, M., JOHNSTON, K., HARRIS, B., LI, Q., FANG, H., COSTELLO, P., SEIBERT, S., and MARTIN, M. *Final Report-Aquifer Storage and Recovery of Potable Water in the Leederville Aquifer*, CSIRO: Water for a Healthy Country National Research Flagship, Australia (2013)

[6] SALIMI, S. and GHALAMBOR, A. Experimental study of formation damage during underbalanced-drilling in naturally fractured formations. *Energies*, **4**(10), 1728–1747 (2011)

[7] ARAB, D., POURAFSHARY, P., AYATOLLAHI, S., and HABIBI, A. Remediation of colloid-facilitated contaminant transport in saturated porous media treated by nanoparticles. *International Journal of Environmental Science and Technology*, **11**(1), 207–216 (2014)

[8] FREITAS, A. M. and SHARMA, M. M. Detachment of particles from surfaces: an AFM study. *Journal of Colloid and Interface Science*, **233**(1), 73–82 (2001)

[9] BERGENDAHL, J. A. and GRASSO, D. Mechanistic basis for particle detachment from granular media. *Environmental Science & Technology*, **37**(10), 2317–2322 (2003)

[10] BRADFORD, S. A., TORKZABAN, S., and SHAPIRO, A. A theoretical analysis of colloid attachment and straining in chemically heterogeneous porous media. *Langmuir*, **29**(23), 6944–6952 (2013)

[11] ELIMELECH, M., GREGORY, J., JIA, X., and WILLIAMS, R. A. *Particle Deposition and Aggregation*, Butterworth-Heinemann, Boston (1995)

[12] KALANTARIASL, A., FARAJZADEH, R., YOU, Z., and BEDRIKOVETSKY, P. Nonuniform external filter cake in long injection wells. *Industrial & Engineering Chemistry Research*, **54**(11), 3051–3061 (2015)

[13] BEDRIKOVETSKY, P., SIQUEIRA, F. D., FURTADO, C. A., and SOUZA, A. L. S. Modified particle detachment model for colloidal transport in porous media. *Transport in Porous Media*, **86**(2), 353–383 (2011)

[14] YANG, Y., SIQUEIRA, F. D., VAZ, A. S., YOU, Z., and BEDRIKOVETSKY, P. Slow migration of detached fine particles over rock surface in porous media. *Journal of Natural Gas Science and Engineering*, **34**, 1159–1173 (2016)

[15] MAHANI, H., BERG, S., ILIC, D., BARTELS, W. B., and JOEKAR-NIASAR, V. Kinetics of low-salinity-flooding effect. *SPE Journal*, **20**(1), 8–20 (2015)

[16] YOU, Z., BEDRIKOVETSKY, P., BADALYAN, A., and HAND, M. Particle mobilization in porous media: temperature effects on competing electrostatic and drag forces. *Geophysical Research Letters*, **42**(8), 2852–2860 (2015)

[17] YOU, Z., YANG, Y., BADALYAN, A., BEDRIKOVETSKY, P., and HAND, M. Mathematical modelling of fines migration in geothermal reservoirs. *Geothermics*, **59**, 123–133 (2016)

[18] YANG, Y. and BEDRIKOVETSKY, P. Exact solutions for nonlinear high retention-concentration fines migration. *Transport in Porous Media*, **119**(2), 351–372 (2017)

[19] GALAGUZ, Y. and SAFINA, G. Modeling of fine migration in a porous medium. *In MATEC Web of Conferences*, **86**, 03003 (2016)

[20] BORAZJANI, S., BEHR, A., GENOLET, L., VAN DER NET, A., and BEDRIKOVETSKY, P. Exact solutions for nonlinear high retention-concentration fines migration. *Transport in Porous Media*, **116**(1), 213–249 (2017)

[21] KREHL, P. O. The classical Rankine-Hugoniot jump conditions, an important cornerstone of modern shock wave physics: ideal assumptions vs. reality. *The European Physical Journal H*, **40**(2), 159–204 (2015)

[22] OCHI, J. and VERNOUX, J. F. Permeability decrease in sandstone reservoirs by fluid injection: hydrodynamic and chemical effects. *Journal of Hydrology*, **208**(3/4), 237–248 (1998)

[23] CHEQUER, L., VAZ, A., and BEDRIKOVETSKY, P. Injectivity decline during low-salinity waterflooding due to fines migration. *Journal of Hydrology*, **165**, 1054–1072 (2018)

[24] OLIVEIRA, M. A., VAZ, A. S., SIQUEIRA, F. D., YANG, Y., YOU, Z., and BEDRIKOVETSKY, P. Slow migration of mobilised fines during flow in reservoir rocks: laboratory study. *Journal of Petroleum Science and Engineering*, **122**, 534–541 (2014)

[25] BEDRIKOVETSKY, P., YOU, Z., BADALYAN, A., OSIPOV, Y., and KUZMINA, L. Analytical model for straining-dominant large-retention depth filtration. *Chemical Engineering Journal*, **330**, 1148–1159 (2017)

[26] RUSSELL, T. and BEDRIKOVETSKY, P. Colloidal-suspension flows with delayed fines detachment: analytical model & laboratory study. *Chemical Engineering Science*, **190**, 98–109 (2018)

[27] SHARMA, M. M. and YORTSOS, Y. C. Transport of particulate suspensions in porous media: model formulation. *AIChE Journal*, **33**(10), 1636–1643 (1987)

[28] BEDRIKOVETSKY, P. Upscaling of stochastic micro model for suspension transport in porous media. *Transport in Porous Media*, **75**(3), 335–369 (2008)

[29] GROLIMUND, D., BARMETTLER, K., and BORKOVEC, M. Release and transport of colloidal particles in natural porous media: 2, experimental results and effects of ligands. *Water Resource Research*, **37**(3), 571–582 (2001)